Magnetism of Alkalitetrafluoromanganates(III) $AMnF_4$ (A = K, Rb, Cs): Neutron Diffraction, Mössbauer and Magnetization Investigations

Michel Molinier, Christoph Frommen, Werner Massa, and Jürgen Pebler

Fachbereich Chemie und Wiss. Zentrum für Materialwissenschaften der Philipps Universität, D-35043 Marburg, Germany

Thierry Roisnel

Laboratoire Léon Brillouin, C.E. Saclay, F-91191 Gif-sur-Yvette Cedex, France

Z. Naturforsch. **48a**, 1054–1072 (1993): received September 17, 1993

The magnetic properties of the d^4 Jahn-Teller systems $A^{I}Mn^{III}F_4$ with layered structures were investigated. *Neutron diffraction* on powders of $KMnF_4$ and $RbMnF_4$ revealed different antiferromagnetic spin arrangements below $T_N = 4.5$ K and 2.3 K, respectively: for $KMnF_4$ canted antiparallel along a and b, for $RbMnF_4$ parallel along a and antiparallel along b, in both cases parallel along c, the stacking direction of layers. *Mössbauer investigations* on ^{57}Fe doped $KMnF_4$ confirmed a spin orientation approximately within the layer plane. A discussion is given of the contributions to the magnetic hyperfine field and the Mössbauer linewidth in quasi-two-dimensional antiferromagnets with Ising anisotropy due to thermal excitation of domain wall dynamics (solitons). The experimental data seem to confirm the predicted exponential temperature dependence of the linewidth. From *magnetization measurements* on powders and a single crystal of $KMnF_4$ the 2-d exchange energy and the out-of-plane and in-plane anisotropies could be extracted. In addition, from susceptibility measurements the exchange energies of $NaMnF_4$, $RbMnF_4$ and $CsMnF_4$ were calculated. A linear dependence of these exchange energies (positive for ferromagnetic $CsMnF_4$, negative for the other $AMnF_4$ compounds) on the $\cos^2$ of the Mn–F–Mn bridge angle is observed and compared with the behaviour of the $AFeF_4$ compounds which is also linear but with reverse sign of the slope. The specific superexchange mechanisms active in Jahn-Teller systems with antiferrodistortively ordered layers are suggested to be responsible for these findings.

Key words: Neutron diffraction; Mössbauer effect; Magnetization; Exchange and anisotropy energy

Introduction

The alkalitetrafluoromanganates(III) are interesting model compounds for the study of magnetic exchange interactions because their $TlAlF_4$-related layered structures exhibit pronounced antiferrodistortive Jahn-Teller ordering and show, in addition, a wide range of Mn–F–Mn bridging angles. Powder samples of $A^{I}Mn^{III}F_4$ (A = K, Rb, Tl, Cs, NH_4) have been investigated 15 years ago [1], but only recently most structures of these compounds have been determined in detail by single crystal X-ray diffraction: $LiMnF_4$ [2], $CsMnF_4$ [3, 4], $NaMnF_4$ [5], $TlMnF_4$ [6], $KMnF_4$ [4] and $RbMnF_4$ [4]. The magnetic structure, determined by neutron diffraction measurements at low temperature, is known for $CsMnF_4$ [3] $NaMnF_4$ [5] $TlMnF_4$ [6]. The most striking feature in this series of layered compounds is that, although all structures show similar antiferrodistortive Jahn-Teller ordering, the magnetism switches from ferromagnetism in $CsMnF_4$ [3] to antiferromagnetism, e.g. in $KMnF_4$ [1]. The determining influence of the Mn–F–Mn angle, governed by the size of the alkali counter cations, on the magnetic exchange energies has already been verified for 1-d antiferromagnetic linear chain compounds $A_2Mn^{III}F_5(H_2O)$ [7]. In the 2-d system $AMn^{III}F_4$, the decrease of the bridging angle Mn–F–Mn even leads to a change in sign of the exchange integral. The main purpose of our investigations on $KMnF_4$ and $RbMnF_4$ presented here was to elucidate the magnetic properties and structures in the interesting intermediate range between antiferromagnetic and ferromagnetic layers and, hence, to close the gap in the magnetic data for the $AMnF_4$ compounds. A survey on the correlations of the structural and magnetic features with varying bridge angles is expected to provide some deeper insight into the possible exchange pathways on an experimental basis.

Reprint requests to Prof. Dr. J. Pebler, Wiss. Zentrum für Materialwissenschaften FB Chemie, Universität Marburg, D-35043 Marburg.

0932-0784 / 93 / 1100-1054 $ 01.30/0. – Please order a reprint rather than making your own copy.

Experimental

Synthesis

The powder samples of $KMnF_4$ and $RbMnF_4$ for neutron diffraction and magnetic measurement (as well as of $CsMnF_4$ for magnetic investigations only) were prepared by solid state reaction of a stoichiometric mixture of AF and MnF_3 in a sealed platinum tube at 520–550 °C. The powder sample of $KMn_{0.99}{}^{57}Fe_{0.01}F_4$ for Mössbauer study was prepared in a similar way with a 1:1 mixture of $Mn_{0.98}{}^{57}Fe_{0.02}F_3$ and MnF_3. The doping of MnF_3 with ^{57}Fe has been achieved by precipitation of $NH_4Mn_{0.98}{}^{57}Fe_{0.02}F_3$ from aqueous HF solution and fluorination to $Mn_{0.98}{}^{57}Fe_{0.02}F_3$ [8]. The single crystals of $KMnF_4$ for magnetic measurements were obtained by reaction of KF with MnF_3 at 800 °C.

Neutron Diffraction

The studies were performed at the Laboratoire Léon Brillouin in Saclay (France), which uses neutron beams from the Orphée reactor. The room temperature data were collected on the high resolution two-axis diffractometer 3T2. The neutron wavelength was 1.2268 Å. The magnetic neutron diffraction studies were carried out on the two-axis G4.1 diffractometer ($\lambda = 2.426$ Å), equipped with a 800 cell linear multidetector, extending over a range of 80 degrees in 2θ. The neutron patterns were recorded at 1.6, 3.3, 4.2, 4.9, 5.5, 6.0, 8.1 K for $KMnF_4$, and 1.5, 2.0, 2.08, 2.15, 2.3, 2.4, 2.55, 3.8, 5.0 K for $RbMnF_4$. The data were refined using a Rietveld analysis method [9] with Gaussian peak shapes. The calculations were performed with the program Young [10] for the nuclear structures and the program Fullprof [11] for the magnetic structures. The neutron scattering lengths have been taken from [12], and the magnetic form factors were extracted from the calculations of Lisher and Forsyth [13].

Mössbauer Experiments

The ^{57}Fe Mössbauer effect was measured between 1.6 K and room temperature in Marburg with a conventional constant-acceleration spectrometer using a 20 mCi ^{57}Co in Rh source. The apparatus has been described in [14].

Magnetic Measurements

Magnetic measurements on powders and on a single crystal were carried out in Marburg on a SQUID magnetometer (Quantum Design). The single crystal was positioned parallel to the three crystallographic axes using X-ray Buerger photographs. An external magnetic field in the range $-55 < H < 55$ kG could be adjusted with a precision of 0.1% by means of a superconducting coil. The sensibility of the magnetization measurement in a magnetic field of $H = 1$ kG was $\Delta M = 2 \cdot 10^{-7}$ G [15].

Neutron Diffraction on $KMnF_4$

Nuclear Structure

As the single crystal X-ray investigations [4] were performed on a pseudomerohedrally twinned crystal, high resolution neutron data on powder were recorded at room temperature to control the lattice constants and atomic parameters. Based on these data, the monoclinic cell constants were refined to $a = 770.62$ (4), $b = 765.71$ (4), $c = 578.89$ (3) pm and $\beta = 90.625$ (3)°. The maximum difference between these parameters and those given by X-ray diffraction was 0.3%. The profile analysis showed the existence of an impurity in our sample, namely $KMnF_3$ (about 3%). Hence, both $KMnF_4$ and $KMnF_3$ were taken into account in the structure refinement. This led, for 939 reflections (2θ range: 10–110°) and 46 parameters to the following reliability factors: $R_p = 4.14$, $R_{wp} = 5.25$, $R_{exp} = 8.2$ and $\chi^2 = 0.410$. For $KMnF_4$: $R_B = 6.83$ and $R_F = 5.20$; for $KMnF_3$: $R_B = 10.77$ and $R_F = 8.69$. The atomic parameters and isotropic temperature factors for $KMnF_4$ are listed in Table 1. They confirm the results of our X-ray investigation on a twinned crystal [4].

Table 1. Atomic parameters and equivalent isotropic temperature factors of $KMnF_4$ and $RbMnF_4$ in the space group $P2_1/a$, $Z = 4$

Atom	x	y	z	U_{eq}
K	0.2475 (9)	0.3042 (7)	0.4862 (9)	0.021 (1)
Rb	0.2473 (7)	0.2894 (4)	0.4803 (6)	0.020 (1)
Mn1	0.0	0.0	0.0	0.008 (1)
	0.0	0.0	0.0	0.007 (2)
Mn2	0.5	0.0	0.0	0.013 (2)
	0.5	0.0	0.0	0.011 (2)
F1	0.2342 (5)	−0.0189 (4)	0.0956 (6)	0.019 (1)
	0.2335 (6)	−0.0142 (5)	0.0788 (7)	0.022 (1)
F2	−0.0648 (5)	−0.0589 (5)	0.2896 (7)	0.018 (1)
	−0.0510 (5)	−0.0517 (7)	0.2853 (6)	0.015 (1)
F3	0.5024 (5)	0.2327 (5)	0.1157 (6)	0.018 (1)
	0.5002 (6)	0.2337 (6)	0.0919 (7)	0.014 (1)
F4	0.5548 (4)	−0.0759 (5)	0.2879 (6)	0.015 (1)
	0.5442 (6)	−0.0637 (7)	0.2845 (7)	0.017 (1)

Magnetic Structure

The neutron diffraction pattern in the paramagnetic phase at $T = 8.1$ K presents only nuclear contributions and is in good agreement with the monoclinic crystal structure determined at room temperature. In our $KMnF_3$, impurity phase transitions occur at 186 K and in the temperature range 89–92 K, according to [16]. Therefore we assume that our study of $KMnF_4$ in the range 1.6–8.1 K was not disturbed by the presence of traces of $KMnF_3$. The cell parameters for $KMnF_4$ at $T = 8.1$ K are the following: $a = 766.7\,(3)$, $b = 761.4\,(3)$, $c = 573.1\,(2)$ pm, and $\beta = 90.55\,(1)°$. With decreasing temperature, additional peaks appear which can be indexed in the monoclinic unit cell. The thermal evolution of some magnetic Bragg peak intensities is shown in Fig. 1 and leads to a magnetic ordering temperature (Néel temperature of $T_N = 4.5 \pm 0.1$ K. In the monoclinic unit cell, the Mn^{3+} ions have the following positions: Mn1: 0 0 0, Mn2: ½ ½ 0, Mn3: ½ 0 0, Mn4: 0 ½ 0. An integrated intensities analysis shows that in the ordered magnetic state the arrangement of the magnetic moments is

along x: $M_{1x} + M_{2x} - M_{3x} - M_{4x}$,

along y: $M_{1y} - M_{2y} - M_{3y} + M_{4y}$,

along z: $M_{1z} + M_{2z} + M_{3z} + M_{4z}$.

A refinement of the magnetic structure at $T = 1.6$ K (2θ range: 15.03–82.93°) was carried out with the program FULLPROF [11]. The 2θ ranges 61.0–65.0° and 72.60–74.85° were excluded because of the presence of broad peaks due to the sample environment. The observed and calculated patterns are shown in Figure 2. The reliability factor R_{Magn} is 5.89% for 49 reflections. The resulting moment is $M = 3.06\,(3)$ μ_B per Mn atom, with following components: $M_x = 2.99\,(3)$, $M_y = 0.49\,(4)$, $M_z = 0.45\,(11)$ μ_B. This means that the spins take an in-plane angle $\alpha_1 \approx 9.3°$ with the a-axis and an out-of-plane angle $\alpha_2 \approx 8.5°$ with the layer. In other words, the moments are more or less lying within the layer. It has to be mentioned, anyhow, that alternative models for the magnetic structure with a different pattern of signs for the M_z component or with an interchange of M_x and M_y contributions (leading to a magnetic structure rotated by 90° around the c direction) gave R_{Magn} values not much worse than the model shown in Figure 16. Thus it seems possible that, due to the tetragonal pseudosymmetry, a magnetic domain structure may be present with alternative a- or b-axis as the "easy" direction. The spin canting pattern may be falsified by this effect. The principal feature of antiferromagnetic order of spins lying approximately within the a,b-plane remains nevertheless unaffected (see discussion below).

Neutron Diffraction on $RbMnF_4$

Nuclear Structure

Morón et al. [17, 18], reported an orthorhombic cell and the space group Pmab for $RbMnF_4$. However, we refined our room temperature neutron diffraction powder data starting from the results of our X-ray structure determination on single crystal [4, 19], i.e. with a monoclinic cell and in the space group $P2_1/a$, the same as for $KMnF_4$. Meanwhile Morón et al. have described the structure of $RbMnF_4$ in this space group as well [20, 21]. The unit cell constants were refined to $a = 781.36\,(4)$, $b = 777.48\,(4)$, $c = 604.66\,(3)$ pm and $\beta = 90.775\,(3)°$. The maximum difference between these parameters and those given by X-ray diffraction is 0.1%. Despite the strong absorption effect of Rb encountered at the X-ray single crystal investigation, the atomic parameters found there are in good agreement with those arising from Rietveld refinement of the neutron data. The profile analysis showed, once more, the existence of an impurity in our sample, namely $RbMnF_3$ (about 5%). Therefore both $RbMnF_4$ and $RbMnF_3$ were considered in the structure refinement. This led, for 1012 reflections (2θ range: 8–110°) and 46 parameters to the following reliability factors: $R_p = 5.13$, $R_{wp} = 6.72$, $R_{exp} = 12.84$ and $\chi^2 = 0.274$. For $RbMnF_4$: $R_B = 6.95$ and $R_F = 5.37$; for $RbMnF_3$: $R_B = 5.38$ and $R_F = 4.28$. The atomic parameters and isotropic temperature factors for $RbMnF_4$ are listed in Table 1.

Magnetic Structure

The neutron diffraction pattern in the paramagnetic phase at $T = 5.0$ K presents only nuclear contributions and is in good agreement with the monoclinic crystal structure determined at room temperature. $RbMnF_3$ orders antiferromagnetically below $T_N \approx 83$ K [22] and, hence, did not affect our study of $RbMnF_4$ in the temperature range 1.5–5.0 K. The cell parameters for $RbMnF_4$ at $T = 5.0$ K are the following: $a = 779.0\,(3)$, $b = 772.6\,(3)$, $c = 600.5\,(2)$ pm, and $\beta = 90.67\,(1)°$. With decreasing temperatures additional peaks appear, indexable in the monoclinic unit cell. The thermal evolution of some magnetic Bragg peak intensities is shown

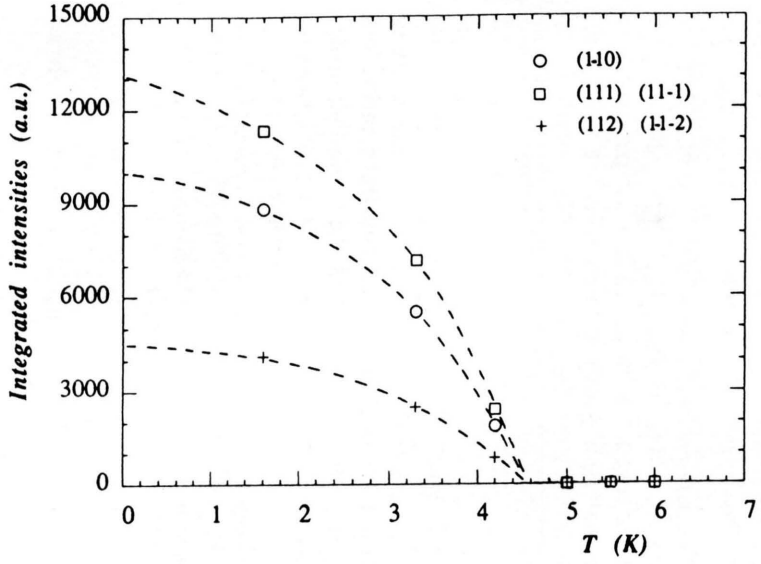

Fig. 1. Temperature dependence of some magnetic peaks of $KMnF_4$.

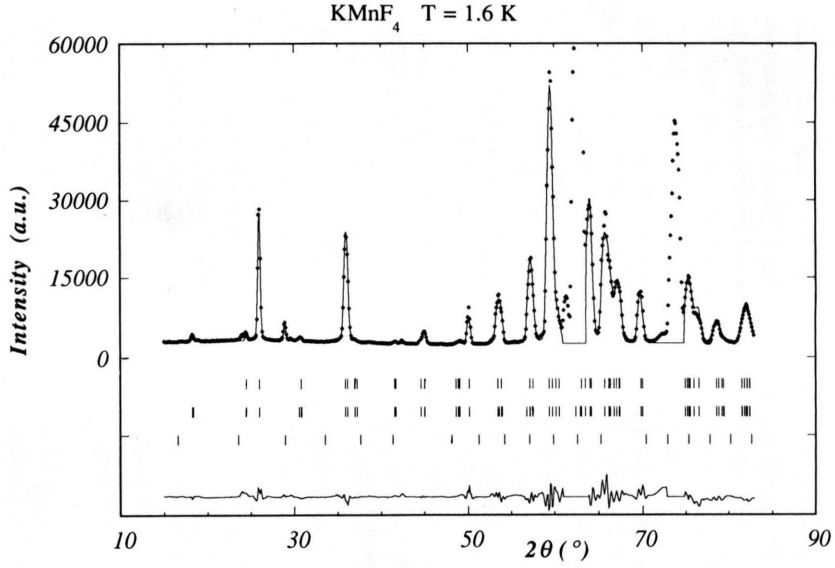

Fig. 2. Observed and calculated nuclear and magnetic intensities at $T = 1.6$ K for $KMnF_4$.

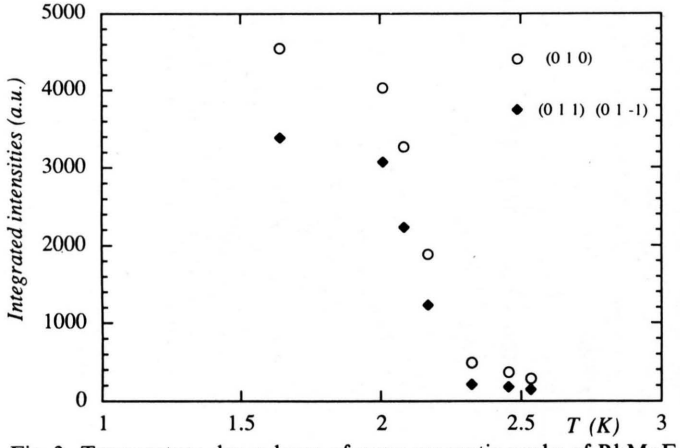

Fig. 3. Temperature dependence of some magnetic peaks of $RbMnF_4$.

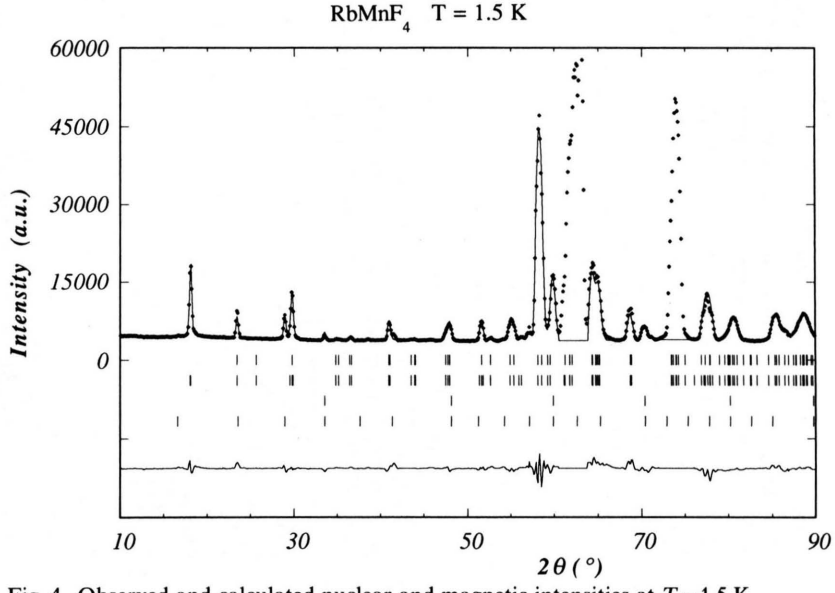

Fig. 4. Observed and calculated nuclear and magnetic intensities at $T = 1.5$ K for $RbMnF_4$.

in Fig. 3 and leads to a magnetic ordering temperature of $T_N \approx 2.3$ K. In the monoclinic unit cell, the Mn^{3+} ions have the same positions as in $KMnF_4$, namely: Mn1: 0 0 0, Mn2: ½ ½ 0, Mn3: ½ 0 0, Mn4: 0 ½ 0. An integrated intensities analysis shows that in the ordered magnetic state the arrangement of the magnetic moments is colinear:

along x: $M_{1x} - M_{2x} + M_{3x} - M_{4x}$,

along y: $M_{1y} - M_{2y} + M_{3y} - M_{4y}$,

along z: $M_{1z} - M_{2z} + M_{3z} - M_{4z}$.

A refinement of the magnetic structure at $T = 1.5$ K (2θ range: 10.03–89.93°) was carried out with the program FULLPROF [11]. The 2θ ranges 60.5–66.0° and 72.0–76.0° were excluded for the same reason as above. The observed and calculated patterns are shown in Figure 4. The reliability factor R_{Magn} is 7.97% for 32 reflections. The resulting moment is $M = 2.47\,(4)\ \mu_B$ per Mn atom, with the following components: $M_x = 1.80\,(5)$, $M_y = 1.42\,(7)$, $M_z = 0.95\,(10)\ \mu_B$. This means that the spins lie rather within the layer than perpendicular to it, with an in-plane angle $\alpha_1 \approx 38°$ with the a-axis and an out-of-plane angle $\alpha_2 \approx 23°$ with the layer. This magnetic structure (Fig. 16) is in good agreement with that reported by Morón et al. * [20, 21]. As for $KMnF_4$, the pseudotetragonal metrics of $RbMnF_4$ prevent a clear discrimination of slightly canted structures suggested by the field dependence of magnetic susceptibilities. Contributions of a magnetic structure generated by 90° rotation around c (or reversion of M_x signs) cannot be excluded.

Mössbauer Study on the Planar Antiferromagnet $KMn_{0.99}{}^{57}Fe_{0.01}F_4$

The $^{57}Fe^{3+}$ ions can be expected to replace the Mn^{3+} ions randomly and to participate in the magnetic order [23]. Between room temperature and 10 K the Mössbauer spectrum of 1% ^{57}Fe in $KMnF_4$ consists of a quadrupole-split pair of absorption lines. The two lines have unequal intensities, that with the lower energy being more intense. The analogous Fe compounds $AFeF_4$ (A = K, Rb, Cs) also show this difference [24–27]; it can be explained by non-random orientation of crystallites in the absorber, since $KMnF_4$ crystals readily cleave in planes perpendicular to the c axis. The particles of powdered $KMn_{0.99}{}^{57}Fe_{0.01}F_4$ tend to line up with their a,b axes parallel to the plane of the absorber. From the intensity difference we can conclude that the lower-energy line is the ($\pm 1/2 \rightarrow \pm 3/2$) line and that the quadrupole splitting for Fe^{3+} in $KMnF_4$ is negative, namely EQ = −1.84 (2) mm/s. This is confirmed by the low-temperature spectra at $T < 6$ K (Figure 5). In the low-temperature range, the ($\pm 1/2 \rightarrow \pm 3/2$) line intensity was corrected by an empirical correction factor derived from the fits above $T_N = 5.5$ (2) K (see next chapter).

Below T_N, the spectra were fitted with a general Hamiltonian of the form

$$\hat{H} = -g\,\mu_N\,\boldsymbol{H}(\theta,\Phi)\,\boldsymbol{I} + (eQV_{zz}/4I(I+1))\,\{I_z^2 - I^2 + (\eta/2)\,(I_+^2 - I_-^2)\}, \quad (1)$$

where θ and Φ are the angles of $\boldsymbol{H}_{hf}$ with respect to the EFG principal axis system. The fits were nearly insensitive to Φ due to the vanishing value of the asymmetry parameter. The quadrupole splitting parameter $EQ = 0.5\,eQV_{zz}\left(1 + \frac{\eta^2}{3}\right)^{1/2}$ was constant within experimental errors throughout the temperature range $1.6\ \text{K} < T < T_N$.

Mössbauer Spectrum at 1.6 K

The parameters obtained for the best fit of the spectrum of $KMn_{0.99}{}^{57}Fe_{0.01}F_4$ at 1.6 K are listed in Table 2 together with the Mössbauer parameters of the analogous planar antiferromagnet $KFeF_4$, well-known from the literature [25]. The analysis of the 1.6 K spectrum yielded that the main axis of the nearly

Table 2. Mössbauer parameters for $KMn_{0.99}{}^{57}Fe_{0.01}F_4$ and $KFeF_4$

	$KMn_{0.99}{}^{57}Fe_{0.01}F_4$	$KFeF_4$
Hyperfine field (kOe)	H_{hf} ($T = 1.6$ K) = 481 (3) H_{hf} (0) = 489 (8)	H_{hf} ($T = 4.2$ K) = 540 (4)
Quadrupole splitting (mm/s)	EQ ($T > 10$ K) = −1.84 (2)	EQ ($T > T_N$) = 1.460 (5)
Isomer shift (mm/s) (relative to iron metal)	IS ($T = 1.6$ K) = 0.420 (8)	IS ($T = 4.2$ K) = 0.54 (1)
Polar angle (°)	$\theta = 61\,(3)$	$\theta = 11\,(2)$
Néel temperature (K)	$T_N = 5.5\,(2)$	$T_N = 145\,(1)$

* In these papers, magnetic structures with spins perpendicular to the layer planes of $KMnF_4$ and $RbMnF_4$, reported earlier by the same authors [18], are revoked

axial symmetric EFG tensor is tilted by an angle $\theta = 61\ (3)^\circ$ with respect to the hyperfine field direction. Interestingly, in the analogous planar structures of $AFeF_4$ (A = K, Rb, Cs) the axial symmetric EFG tensor is oriented along the terminal Fe–F bonds [24–28]. If we also assume for $KMn_{0.99}{}^{57}Fe_{0.01}F_4$ an orientation of V_{zz} parallel to the terminal (Mn, Fe)–F bonds, i.e. a mean angle of 25.2° with respect to the *c*-axis [4], then we obtain the magnetic hyperfine field direction at angles between 36° and 86° with the *c*-axis. This means that the moments in $KMn_{0.99}{}^{57}Fe_{0.01}F_4$ can lie approximately within the layer, confirming the present results ($\approx 81^\circ$) of neutron diffraction studies, whereas in the Fe-layered structures, they are perpendicular to the layers. The isomer shift $\delta = 0.42$ mm/s (relative to iron metal) is characteristic for Fe^{3+}, even though it is smaller than $\delta = 0.55$ mm/s that is given for the $AFeF_4$ compounds [25–27]. The quadrupole splitting of about -1.80 mm/s is big for Fe^{3+} in a fluorine compound, but is similar in magnitude to that observed in the analogous layer structure compound $KFeF_4$ (Table 2). The higher value of the quadrupole splitting for $KMn_{0.99}{}^{57}Fe_{0.01}F_4$ can be explained by the distortion of the Fe^{3+} octahedra and shortening of equatorial bonds induced by the neighbouring Jahn-Teller distorted Mn^{3+} octahedra (see below).

The temperature dependence of the Mössbauer spectra is shown in Figure 5. The value of the Néel temperature in $KMnF_4$, determined by independent measurements, is $T_N = 5.5\ (5)$ K.

We have analysed the Mössbauer spectra with symmetric Lorentzian lines. The temperature range can be divided into three parts. At temperatures between 9 and 7 K a temperature-dependent asymmetry of the absorption lines was observed. As the temperature was further decreased, the spectra showed the coexistence of contributions from the paramagnetic and magnetically ordered phases between 6 and 4.8 K. Additionally, the transition to the magnetically split phase was observed by strong broadening of the lines. Below 4.5 K the line widths returned to normal. A pure combined hyperfine pattern was observed that showed an increasing splitting towards lower temperature.

On calculating the temperature dependence of the sublattice magnetization using simple spinwave theory for two dimensions [29] we found a good agreement between the experimental data of H_{hf} and the spinwave theory $H(T) = H_0\{1-(0.0587/4S)(T/2JS)^{3/2}\}$ for a quadratic layer at temperatures $T < T_N$. In fitting the data of H_{hf} to the spin-wave theory, an estimation of the saturation field $H_{hf}(0) = 489\ (5)$ kOe and of the exchange energy $J/k = -0.5\ (2)$ K were obtained. This simple spin-wave approximation does not take into account the local anisotropy constant D as well as the zero-point spin reduction ΔS. The latter parameter is of significance in a low-dimensional antiferromagnetic compound because a perfectly aligned Néel state is not an eigenstate of the antiferromagnetic exchange Hamiltonian [30], except in the case where its anisotropy is infinite. Consequently, even at $T = 0$ K, the spins will be subject to deviations. On the basis of the spin wave theory, ΔS varies roughly from 0 for $D \to \infty$ to $1/2z$ for $D = 0$, where z means the number of immediate neighbours [31]. The sublattice magnetization will be reduced to $M = g\mu_B H(S - \Delta S)$. This spin reduction $(S - \Delta S)/S$, which is according to Johnson [32] equal to H/H_0- where H_0 is the saturation value of H_{hf} for the high-spin Fe^{3+} ion in FeF_3- amounts to about 16% for the planar antiferromagnet $KFeF_4$ which is in excellent agreement with theoretical predictions from spin-wave and perturbation theory [31]. If we assume as in [33] $H_0 = 624$ kOe ($\Delta S/S = 3\%$), the value of $H_{hf}(0) = 489$ kOe for $KMn_{0.99}{}^{57}Fe_{0.01}F_4$ corresponds to 24% spin reduction. This value, which can be directly taken from the Mössbauer experiment, is too large. As an explanation for this physically dubious result, as is discussed in the literature [31], one can suggest that there exists a transfer of unpaired electron spin from the magnetic Mn^{3+} ion to its nearest magnetic Fe^{3+} neighbours via the intervening ligand. Such a process, known as super-transferred hyperfine interactions, will reduce the ^{57}Fe splitting of the nuclear energy levels and thus the value of H. In addition, covalency likewise reduces the magnetic hyperfine field since a small part of the electrons delocalizes from neighbouring fluorine ligands onto the paramagnetic ions between them. This may be important in $KMn_{0.99}{}^{57}Fe_{0.01}F_4$ because in $KFeF_4$ a slightly compressed octahedron is found with four similar bridgeing Fe–F bonds (average of 196.8 pm) and two short terminal bonds (187.6 pm). In comparison with that, the structural matrix of $KMnF_4$ shows remarkably shortened terminal bonds (180.4 pm) and asymmetrical M–F–M briges with a shorter (188.1 pm) and a very long bond (215.6 pm). From the ligand field spectra of mixed crystals $(NH_4)_2Mn_{1-x}Fe_xF_5$ [34] it could be deduced that in a Mn–F–Fe bridge, where Fe competes for the bridg-

ing F-ligand with an Mn–F bond weakened by the Jahn-Teller effect, the Fe–F bond gets nearly as strong as a terminal bond. On the other hand, in the other direction of the layer the Fe–F bond competing with a short Mn–F bond (presumably somewhat stronger than Fe–F) will undergo a remarkable lengthening. In the absence of a Jahn-Teller effect, this elongation should be much lower than 215 pm found in MnF_6 octahedra. Taking into account a mean Mn–F distance of 201.5 pm for the asymmetric bridge, the Fe–F bond length could be a little longer than this value. Nevertheless, a local inrease of the bridge angle may compensate partly such an extreme elongation. Hence, we expect a remarkably pseudotetragonal elongated $[FeF_6]$ octahedron with four very short equatorial Fe–F distances (surely below 190 pm) and a long axis of $2x$ about 200 pm. Such very short equatorial bonds are not encountered in pure iron compounds. This may explain the difference in the magnetic hyperfine fields of 540 kOe and 489 kOe observed in $KFeF_4$ and $KMn_{0.99}{}^{57}Fe_{0.01}F_4$, respectively. Taking into account the success of spin-wave theory [31] in describing the properties of 2-d ($S>1$) antiferromagnets, one would conclude that the spin-wave prediction for the Fe^{3+} fluorides $S=16.7\%$ (compared to the experimental value for Fe^{3+} of 16% by Johnson [32] is probably correct and that our experimental results for $KMn_{0.99}{}^{57}Fe_{0.01}F_4$ are distorted by the covalency and super-transferred hyperfine interactions.

Mössbauer Spectra near T_N

As already mentioned, we observe just below und above T_N an unusual (non-Brillouin) behaviour in the temperature dependence of the internal fields. The transition from the magnetically ordered state to the paramagnetic state is obviously accompanied by strong line broadening caused by slow relaxation phenomena. It is clear from this temperature range (Fig. 5–6) that the magnetic hyperfine field does not decrease to zero at T_N and is, therefore, not proportional to the spontaneous magnetization. Additionally, the intensity of the inner quadrupole split pair of absorption lines increases at the cost of the intensity of the magnetically split spectra at T_N. Between 4.8 and 6 K, the Mössbauer experiments on $KMn_{0.99}{}^{57}Fe_{0.01}F_4$ show the superposition of two subspectra in a compound with two nearly identical crystallographic sites. This can be interpreted in terms of a slowly and a fast relaxing subspectrum, whose static Mössbauer parameters are identical. Since H_{hf} is proportional to the electron spin $\boldsymbol{S}$, the fluctuations in H_{hf} can be related to the spin-autocorrelation function $\langle \boldsymbol{S}(0,0)\,\boldsymbol{S}(0,t)\rangle$ [35]. In 3-d magnets, the fluctuations of $\boldsymbol{S}$ in the paramagnetic regime are very rapid compared to the nuclear Larmor frequencies ω_L. This implies that H is proportional to the sublattice magnetization. In quasi 2-d magnets, however, the intraplane correlation lengths can already be substantial at temperatures $T=2\,T_N$, explaining why we have a non Brillouin behaviour, provided the in-plane anisotropy is large.

The possible occurrence of slow spin-spin relaxation may be excluded, since spin-spin relaxation is obviously fast in magnetically concentrated systems. Another possibility like a distribution of Néel temperatures can also be ruled out here on the basis of the performed neutron diffraction and susceptibility experiments (see this paper). Finally, the origin of the broadened asymmetric spectra in the region near critical point is attributed to residual 2-d correlations.

A question of current interest concerns the possibility of localized excitations (solitons) in 2-d magnets. Although the soliton concept has been well established for Heisenberg spin chains, little is known about the situation in 2-d lattices. For the 2-d Heisenberg magnet a static soliton solution has been presented [36] and extended to anisotropic systems [37]. However, it is not yet clear how these solutions will affect the dynamics in detail. Qualitatively, by analogy with the 1-d case, a broadening of the Mössbauer linewidths is expected, which should be proportional to the number of solitons, $n_s \propto \exp(-E_A/kT)$, with E_A being the soliton activation energy. In fact, for several manganese layer compounds, such an Arrhenius law has been observed in the EPR linewidth close to the phase transition [38]. However, until now no manifestation of non-linear excitations was reported for two-dimensional magnetic Fe^{3+} compounds. The spectra of $AFeF_4$ (A = K, Rb, Cs) do not display any temperature-dependent line broadening above the 3-d phase transition. Solitons are present by virtue of the anisotropy, and, since Fe(III) is $3d^5$, the single-ion anisotropy of Fe(III) will be negligible or will probably be smaller than the 3-d ordering energy $k\,T_N$. Mn(III) is $3d^4$ and so should have strong anisotropic properties, which are transmitted via the Mn–Fe exchange to the Fe atoms. The latter become polarized in the same direction as the Mn spins [39]. Adopting

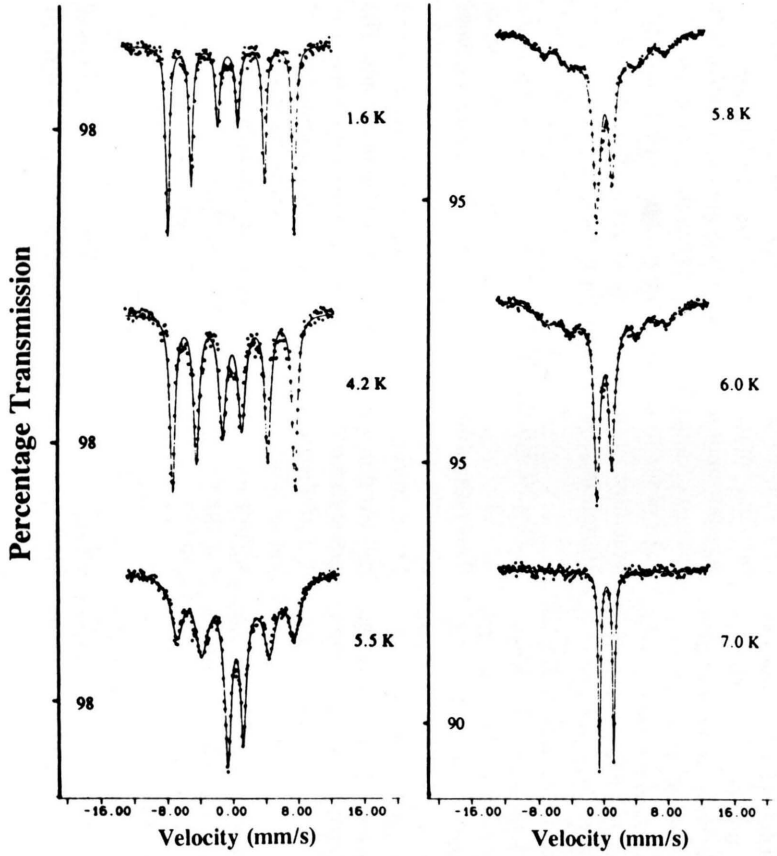

Fig. 5. Temperature dependence of the Mössbauer spectra for $KMn_{0,99}Fe_{0.01}F_4$. The solid lines represent the fit using a sextet and doublet with independent parameters for the linewidths. The averaged results for the linewidth are shown in Figure. 7.

Fig. 6. Temperature dependence of the magnetic hyperfine field and ratio I_D/I_W where I_D is the area of the doublet and I_W is the sum of the areas of the doublet and sextet. The graph of I_D/I_W shows qualitatively the change from 3-d to 2-d magnetic ordering. The solid line represents the $T^{3/2}$ law of the spin wave approximation.

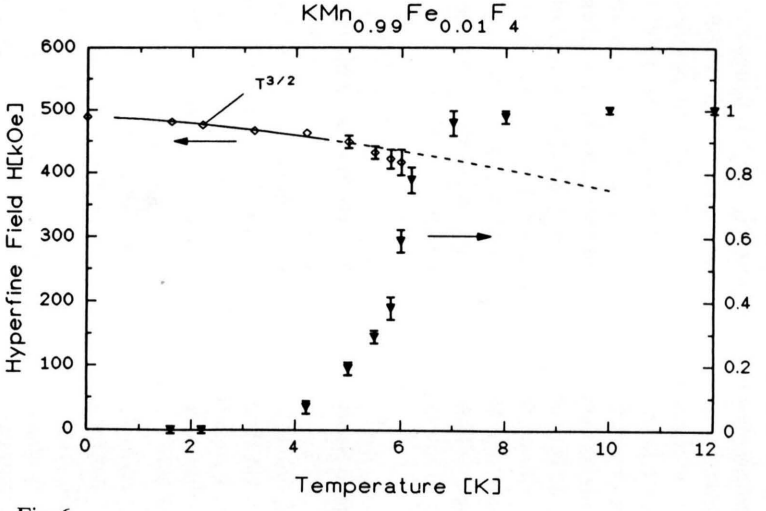

Fig. 6.

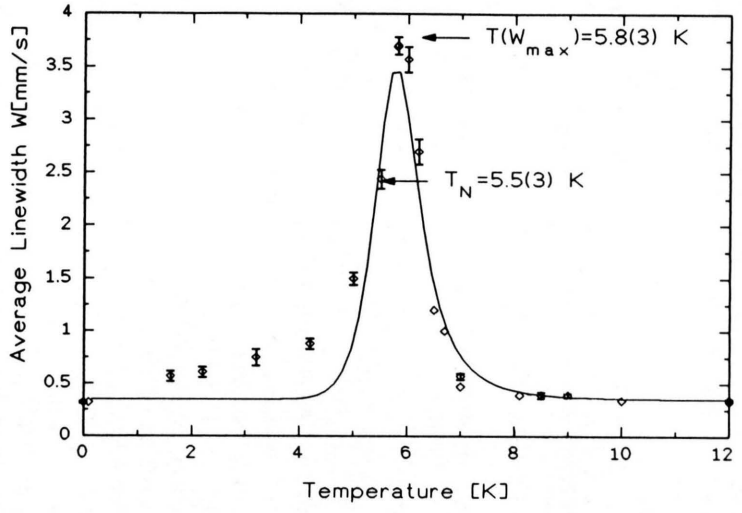

Fig. 7. Experimental linewidth W versus temperature. The solid curve represents the calculated behaviour according to (2).

a similar soliton concept as established for anisotropic chains, the line broadening in the spectra of $KMn_{0.99}{}^{57}Fe_{0.01}F_4$ was analyzed by the expression [40]

$$W(T) = \frac{\omega_L^2 G_\omega}{G_\omega^2 + 0.5\,\omega_L^2} + W_{nat}\,, \tag{2}$$

where G_ω means the flip-rate of the electron spin:

$$G_\omega = G_0 \exp\{-E_A/kT\}\,. \tag{3}$$

Further, ω_L is the average nuclear Larmor frequency of $0.5 \cdot 10^8$ Hz for $H_{hf} = 489$ kOe, and E_A is the soliton activation energy:

$$E_A = 2\pi S^2 (DJ)^{1/2}\,, \tag{4}$$

where D and J are the in-plane (Ising-type) anisotropy and in-plane exchange energy, respectively. For $G > \omega_L$, the line broadening is according to [35] proportional to $\exp\{E_A/kT\}$. In order to estimate the activation energy E_A, we plotted $\ln(W)$ versus $1/T$ and calculated from the slope the activation energy $E_A/k = 31$ (5) K for $KMn_{0.99}{}^{57}Fe_{0.01}F_4$ in the temperature range $T_N < T < 10$ K. Finally, we fitted (2) and (3) to the measured halfwidths $W(T)$ for $T > T_N$. We found by a least squares fit $E_A/k = 30$ (5) K, $G_0 = 10^{13}$ Hz and a maximal line broadening of 3.75 mm/s at 5.8 (5) K with fixed $W_{exp} = 0.30$ mm/s. The theory of solitons predicts a maximal line broadening [40] of $W_{exp} + (2\,\omega_L)^{1/2} = 3.5$ mm/s at $G_\omega = \omega_L$. If we assume a precision of about 2% for the linewidths $W(T)$, then from (2) the sensitivity of the Mössbauer effect covers a range between 10^6 and $0.6 \cdot 10^{11}$ s^{-1} [40]. The correlation times calculated from (2) are $0.2 \cdot 10^{-7}$ s, $0.5 \cdot 10^{-8}$ s and $2 \cdot 10^{-10}$ s at temperatures of $T \approx T_N = 5.5$ (3) K, $T = 6.5$ K and 8.5 K, respectively. Above this latter temperature the flip rates of the magnetic moments are outside Mössbauer window. The result is shown in Figure 7. The error bars in the figure represent a combination of the statistical errors in the linewidths indicated in the computer fits and the spreads observed when averaging the halfwidths of the magnetic and quadrupole pattern below and above T_N, respectively.

In order to estimate the in-plane exchange energy J/k we define on the basis of the quadratic Heisenberg model the region $T_N < T < T_u \approx 2.07\,S(S+1)\,J/k$ in which 2-d excitations can be observed. The upper limit T_u of the Mössbauer window corresponds to the temperature where $W = W_{exp}$. Taking $T_u = 8.5$ K we estimate from the relationship of T_u the exchange energy $J/k = -0.68$ (5) K and hence from (4) the in-plane anisotropy energy $D/k = 1.45$ (5) K. The exchange and anisotropy constants may be overestimated, because our calculation does not take into account possible spin correlations beyond T_u. However, the results derived by the upper crude approximations are in excellent agreement with the magnetization studies below. It is also noteworthy that the temperature of the maximum for the linewidth nearly coincides with the observed Néel temperature from magnetic measurements. This result is in agreement with previous results of low-dimensional systems [40, 41].

Magnetic Study of the 2D Antiferromagnet $KMnF_4$

The molar magnetic powder susceptibility calculated from the field dependence of the magnetization is plotted versus temperature in Figure 8. The susceptibility has been corrected for a diamagnetic contribution of $7.4 \cdot 10^{-5}$ cm^3/mole. The broad maximum in the χ versus T curve at about 8.5 K confirms the expected 2-d magnetic properties. At high temperatures ($T > 150$ K) a linear variation of the reciprocal susceptibility is observed with a small θ_p value for the Curie-Weiss temperature of -15 (4) K and a Curie constant of $C = 2.93$ (6) cm^3 K/mole. The experimental value for the magnetic moment $\mu_{Mn} = (8\,C)^{1/2} = 4.83$ (5) μ_B (spin-only value: 4.90 μ_B) is in good agreement with the usual values found in manganese (III) compounds.

In order to calculate the planar antiferromagnetic exchange energy $J < 0$ we consider the interaction Hamiltonian with orthorhombic symmetry

$$\hat{H} = 2J \sum \boldsymbol{S}_i \boldsymbol{S}_j - \sum \{D_x S_{ix}^2 - D_z S_{iz}^2 + g\mu_B \boldsymbol{H} S_i\}\,. \tag{5}$$

The summation (i, j) is over nearest neighbour pairs. Thus the anisotropy constant D_z establishes a planar $(X\,Y)$ anisotropy for the moments whereas D_x singles out the x-axis as the preferential axis within this easy plane (Ising-type anisotropy).

For the quadratic layer Heisenberg antiferromagnet with isotropic exchange Hamiltonian (first term in (5)) we use as an approximation the series expansion for the reciprocal susceptibility

$$\frac{N g^2 \mu_B^2}{2\chi J} = 3B + \sum \frac{C_n}{B^{n-1}}\,, \tag{6}$$

where $B = kT/2JS(S+1)$ and the coefficients C_n (calculated from the formalism [42] are in accordance with

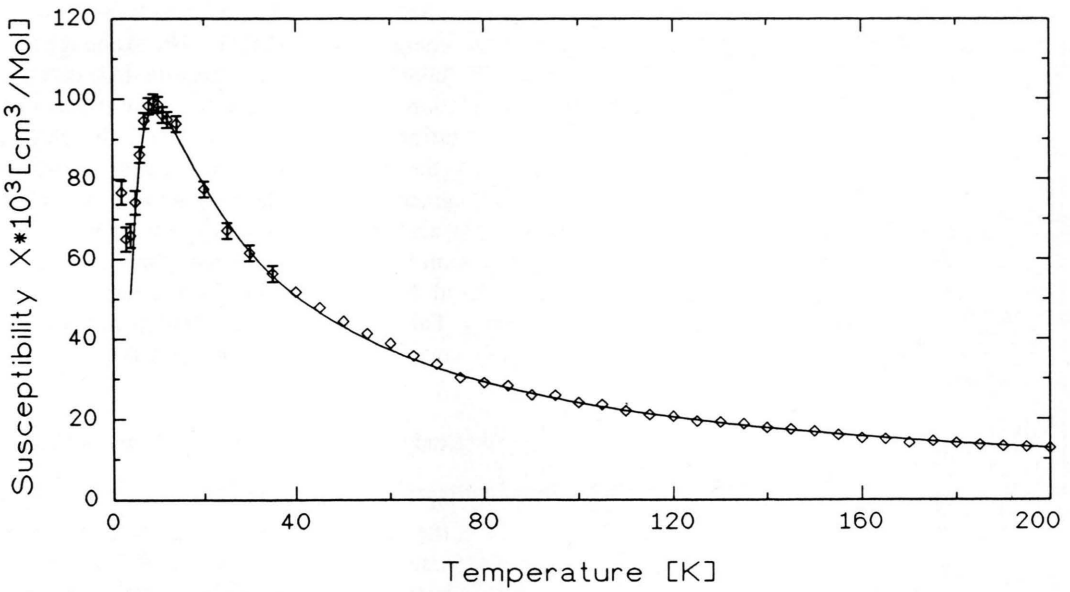

Fig. 8. Magnetic susceptibility for $KMnF_4$. The solid line represents the best fit curve calculated for the quadratic-layer Heisenberg antiferromagnetic according to (6).

Lines [43] $C_1 = 4$, $C_2 = 1.50$, $C_3 = 0.252$, $C_4 = 0.258$, $C_5 = 0.124$, $C_6 = 0.015$. The best fit curve is shown in Fig. 8, yielding parameters, the $g = 1.975$ and $J/k = -0.65$ (2) K. The agreement with the exchange energy $J/k = -0.68$ (5) K derived from our Mössbauer experiments is surprisingly good. The maximum of the calculated magnetic susceptibility occurs at $T(\chi_{max}) = 8.6$ K. For $T > T(\chi_{max})$ the spin correlations vanish and the compound behaves like a normal paramagnet with a Curie-Weiss susceptibility. It is noteworthy that the temperature T_u defined as the upper limit of the Mössbauer window (see preceding chapter) is in excellent agreement with $T(\chi_{max})$.

The discrepancy between theory (6) and experiment for temperatures below $T(\chi_{max})$ is probably due to the existence of a weakly canted rather than a strictly antiferromagnetic spin arrangement below T_N, leading to a divergence of susceptibility at 6 K.

In order to get informations about spin canting and the ordering temperature T_N we used a stack of small single crystals oriented along the *c*-axis, which is perpendicular to the layer. After zero-field cooling we measured the magnetization in the range between 1.8 K and 20 K, warming up and then cooling down again in a weak field of 100 G parallel and perpendicular to the *c*-axis. Figure 9 shows that small canted components of the spins exist parallel to the *c*-axis and within the plane. The different branches of magnetization diverge at 5 K. The inflection points of the magnetization curves may define in the case of a quasi 2-d system [31] the antiferromagnetic ordering temperature as $T_N = 5.5$ (2) K, which is in agreement with $T(W_{max})$ derived from the Mössbauer experiments. The strong evidence of three dimensional long range ordering below this temperature is given from the appearance of hysteresis phenomena and residual magnetization (Figures 10–11).

To derive the anisotropy constants D_x and D_z in (5) we measured the magnetization of a small single crystal (0.57 mg) as function of an external magnetic field and the temperature along the three crystal axes. A field dependence of the magnetic susceptibilities was found below $H = 3$ kG in all directions. The temperature dependence of all three χ curves calculated from $M = \chi H$ displays broad maxima at 8.5 K in agreement with the powder measurements. Different curves for χ_a, χ_b, and χ_c reveal that the magnetic ordering is highly anisotropic. Adopting the results of neutron diffraction, the perpendicular components of zero-field susceptibilities extrapolated for $T \to 0$ are $\chi_b(0) = 92.5 \cdot 10^{-3}$ cm³/mole and $\chi_c(0) = 74.4 \cdot 10^{-3}$ cm³/mole.

The susceptibility, uncorrected with respect to weak ferromagnetism, is shown in Figure 12. The behaviour

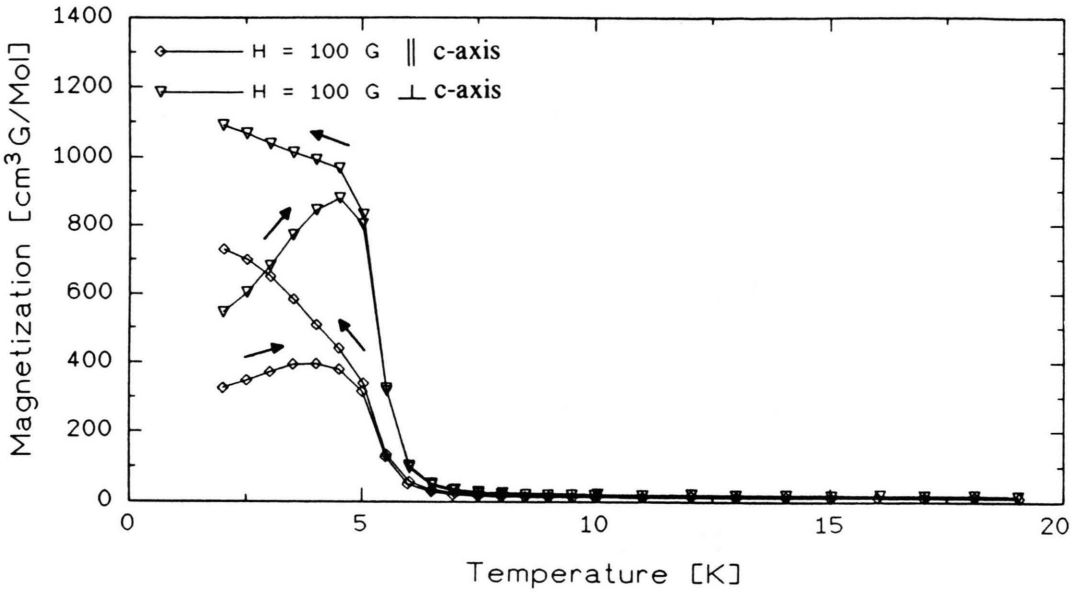

Fig. 9. Magnetization of $KMnF_4$ in a small magnetic field $H = 100$ G.

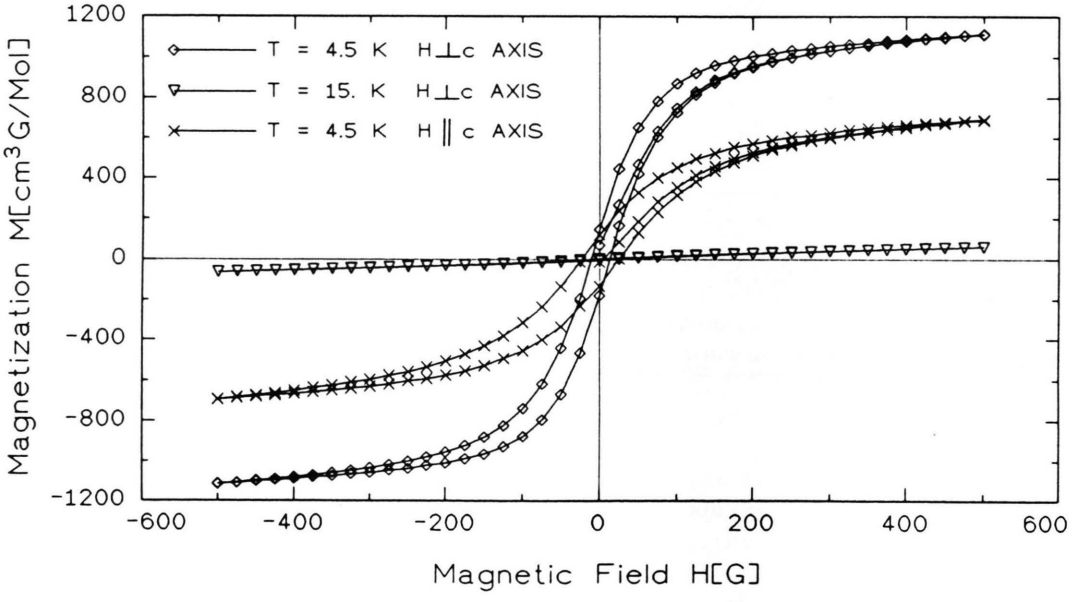

Fig. 10. Magnetization M of $KMnF_4$ for $-600\text{ G} < H < 600\text{ G}$ at 4.5 K and 15 K.

of the magnetic susceptibility in $KMnF_4$ is an example of a 2-d planar Heisenberg antiferromagnet, since the planar anisotropy clearly follows from the fact that above the maximum at 8.5 K, the perpendicular susceptibility χ_b as measured within the easy plane nearly coincides with the parallel susceptibility χ_a, whereas the perpendicular susceptibility χ_c in the direction out of the easy plane is lowered substantially as a consequence of a large planar anisotropy D_z. With the exchange constant J determined above, the susceptibility can be calculated at $T = 0$ from the prediction of the perpendicular susceptibilities from spin wave the-

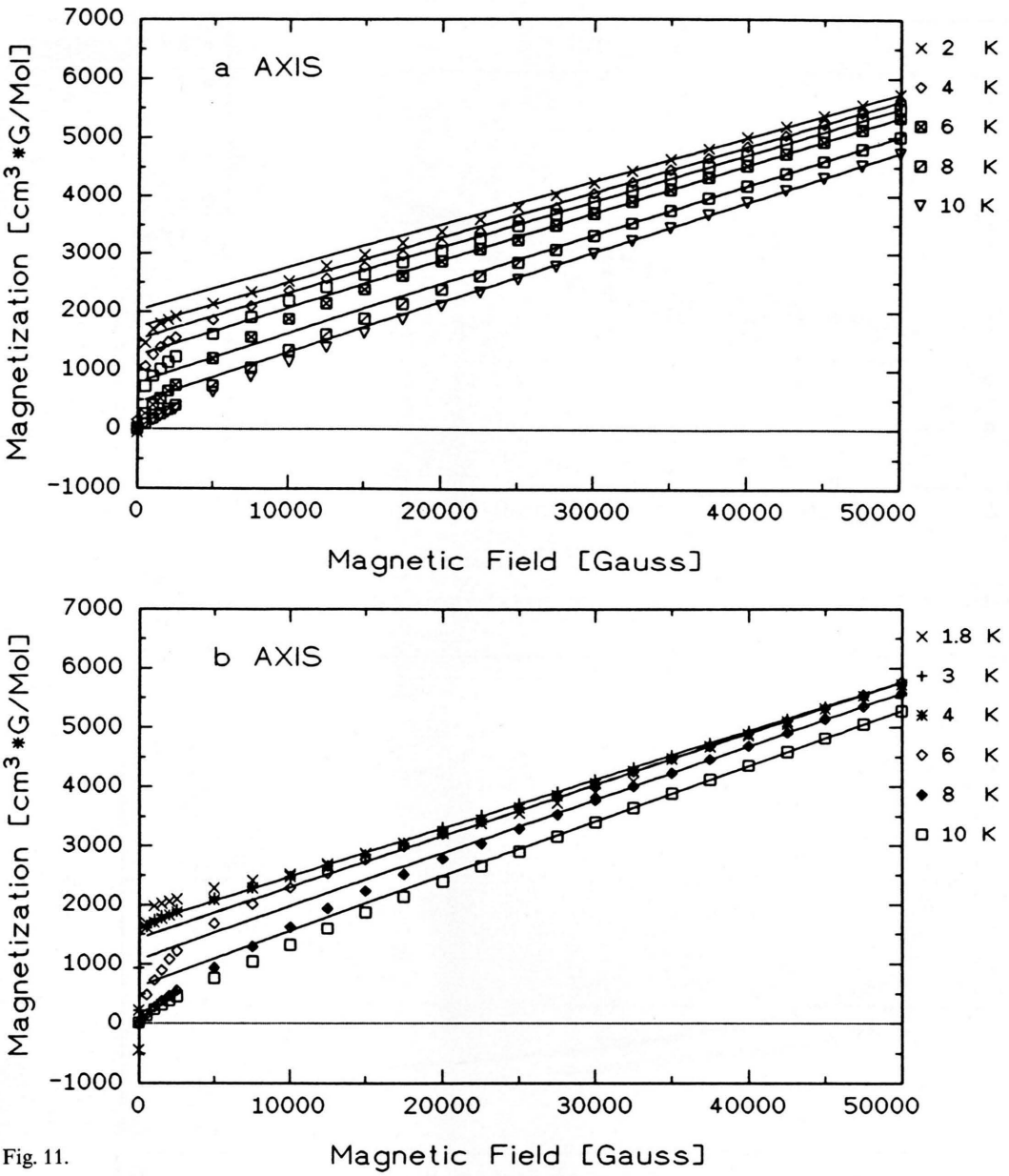

Fig. 11.

ory [30]:

$$\chi_\perp(0) = \frac{\chi_\perp^\circ}{1+\alpha/2}\left\{1 - \frac{\Delta S(\alpha)}{S} - \frac{e(\alpha)}{(2+\alpha)\,zS}\right\}. \qquad (7)$$

In this equation $\chi_\perp^\circ = N g^2 \mu_B^2 / 4zJ$ is the molecular field prediction for the perpendicular susceptibility of an antiferromagnet with $H_A = 0$ and at $T = 0$, z is the number of nearest neighbour Mn^{3+} ions in a layer, and α is the anisotropy parameter $\alpha = H_A/H_E$, where $H_A = 2DS/g\mu_B$ and $H_E = 2zJS/g\mu_B$. The quantities $S(\alpha)$ and $e(\alpha)$ are corrections arising from the effects of zero-point spin deviations. The Mössbauer effect in $KFeF_4$ gives a spin reduction [31] $\Delta S/S$ of 0.16 for an anisotropy constant of $\alpha = 6 \cdot 10^{-3}$. Considering the spin reduction as a function of α as calculated by Colpa et al. [44] we obtain for $KMnF_4$ $S(\alpha)/S = 0.10$. The quantity $e(\alpha)$ is almost independent of α [45], so we use the value $e(0) = 0.632$ given by Keffer and

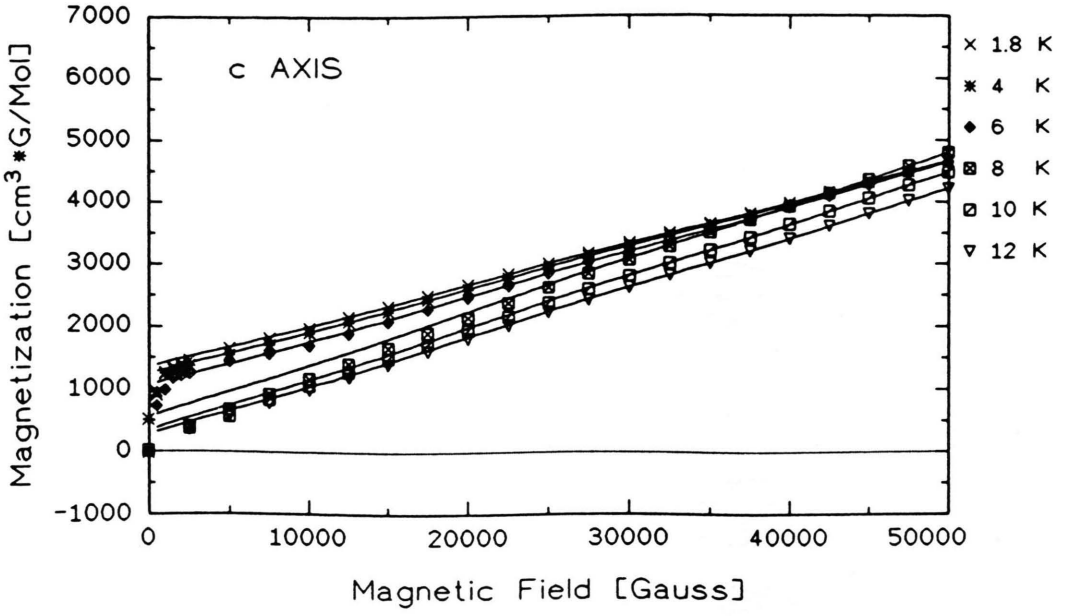

Fig. 11. Magnetization M along the three crystal axes as a function of external magnetic field in $KMnF_4$.

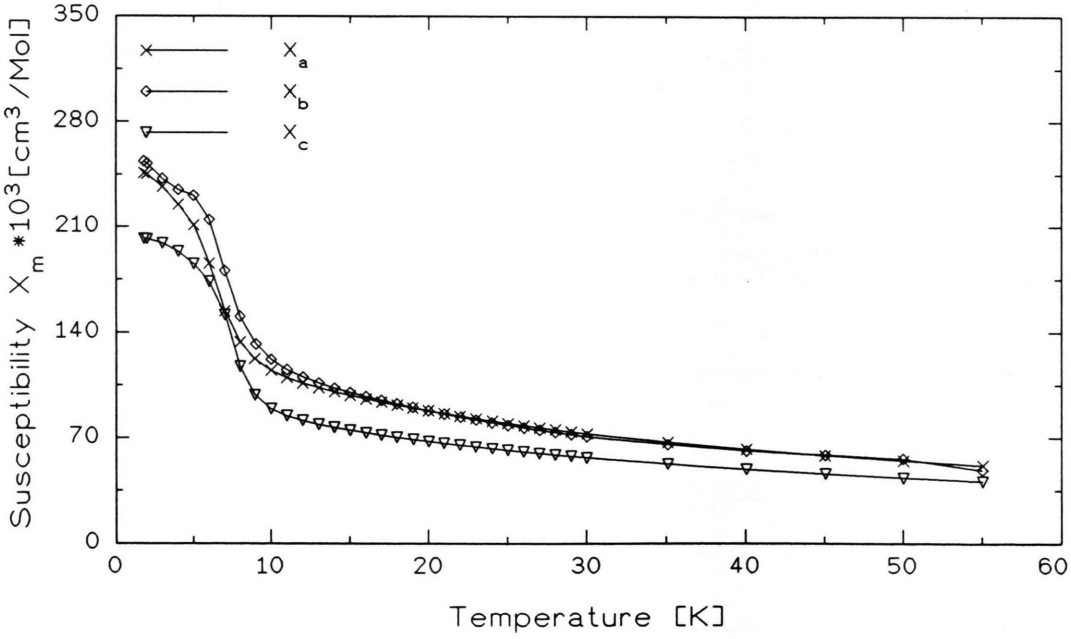

Fig. 12. Magnetic susceptibility X along the three crystal axes as a function of temperature in $KMnF_4$.

Breed [30, 46]. With the experimental values of the perpendicular susceptibilities $\chi_b(0)$ and χ_c (0) (see above) we obtain from (7) the anisotropy parameters $\alpha = 0.65$ and $\alpha = 1.40$, and hence the in-plane anisotropy $D_x/k = 1.7\,(3)$ K and out-of-plane anisotropy $D_z/k = 3.5$ K, respectively.

The exchange interaction $J/k = -0.65$ K for $KMnF_4$ is unusually small. For comparison we put together the characteristic parameters for $KMnF_4$ and from literature [24, 25] the parameters for $KFeF_4$ (Table 3). Listed are the spin value S, the transition temperature T_N, the intralayer exchange J/k, $T(\chi_{max})$,

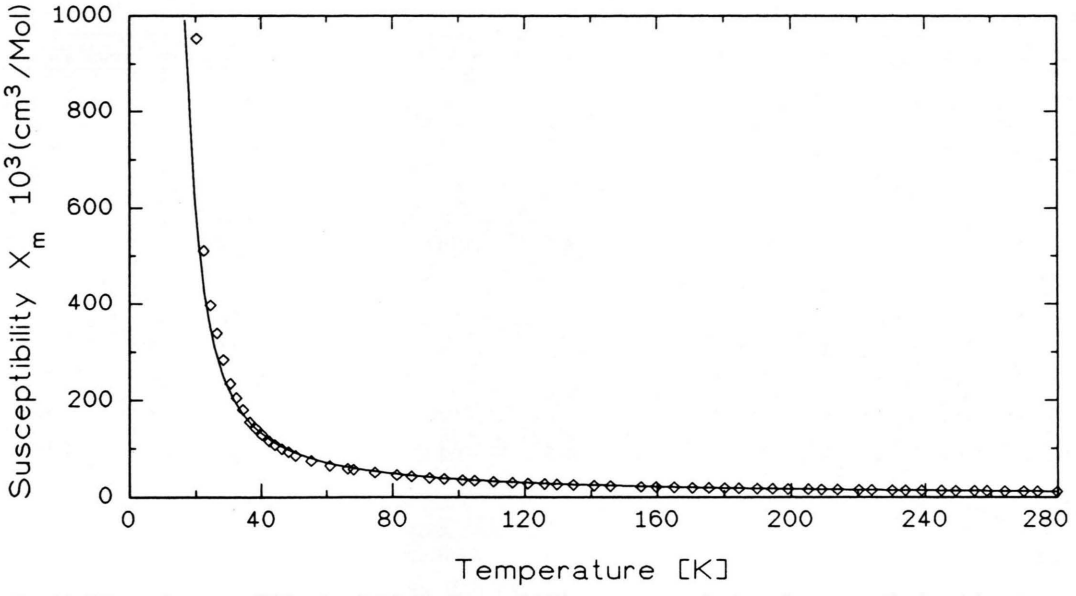

Fig. 13. Magnetic susceptibility for $CsMnF_4$. The solid line represents the best fit curve calculated for the quadratic-layer Heisenberg ferromagnet according to [43].

and two anisotropy values, which apply to the anisotropy within the easy plane and the out-of-plane anisotropy, respectively; additionally, the quantities kT_N/J and T_N/θ_2 are given, where the Curie-Weiss temperatures θ_2 have been calculated from J/k according to the formula: $k\theta_2 = (2/3)\, z\, S(S+1)\, J$.

The values of kT_N/J and T_N/θ_2 approximately agree with the theoretical prediction for the 2-d Heisenberg model. However, although the crystal structures of $KMnF_4$ and $KFeF_4$ are closely related, the exchange energies J/k differ almost by a factor 19. The percentage decrease in $T(\chi_{max})$ and J/k going from $S = 5/2$ to $S = 2$ would only reduce $T(\chi_{max})$ and J/k by 31%.

Exchange Energies of Other $AMnF_4$ Compounds

In this context it was interesting to calculate the two dimensional exchange energies J/k for the already known layer structures of $NaMnF_4$ [5], $RbMnF_4$ and $CsMnF_4$ [4] on the basis of the high temperature approximation for the quadratic Heisenberg model (6). For this purpose we performed new susceptibility measurements on powder samples of $RbMnF_4$ [8] and $CsMnF_4$ (Figure 13). In the case of $NaMnF_4$ we used the values from our earlier measurements [5]. The parameters obtained are reported in Table 4.

Table 3. Comparison of magnetic data for $KMnF_4$ and $KFeF_4$

Parameter	$KMnF_4$	$KFeF_4$
S	2	5/2
T_N (K)	5.5	137
J/k (K)	−0.65	−12.3
$T(\chi_{max})$ (K)	8.6	217
α	0.65/1.40	$6.5 \cdot 10^{-3}$
kT_N/J	8.46	11.1
T_N/θ_2	0.53	0.48

Magnetostructural Correlations in the $AMnF_4$ Series

In contrast to other strong Jahn-Teller systems with layered structures like A_2CuF_4 or A_2CrCl_4 [31, 47], where the M–X–M bridges are near 180°, the fluoromanganates (III) $AMnF_4$ reported here provide a large variation of lower bridge angles from 138° to 162° (Table 4). The local geometry of the elongated $[MnF_6]$ octahedra remains approximately constant, anyhow. In all cases, these groups order in an antiferrodistortive manner (Figure 14). Thus, the Mn–F–Mn bridges are strongly asymmetric with typical bond lengths Mn–F of 215 and 186 pm.

As in this series of $AMnF_4$ compounds, the exchange energies strongly vary with the bridge angles (Table 4), it seems possible to correlate this feature with possible exchange pathways in the structures,

Table 4. Structural and magnetic data of $AMnF_4$ compounds

Compound	Space group	Cell constant (pm, °)	Z	Mn–F (pm) (short)	Mn–F (pm) (long)	Mn–F–M (°)	θ_p (K)	T_N or T_C (K)	g	J/k (K)	Magnetic behavior	Lit.
$LiMnF_4$	$P2_1/c$	$a=$ 541.4 $b=$ 462.9 $c=$ 569.4 $\beta=$ 113.24	2	181.8 186.8	213.7	132.7						[2]
$NaMnF_4$	$P2_1/c$	$a=$ 573.6 $b=$ 489.2 $c=$ 574.8 $\beta=$ 108.07	2	180.8 186.9	216.7	138.4	−19	13	1.99	−1.15	AF	[5, 8]
$KMnF_4$	$P2_1/a$	$a=$ 769.9 $b=$ 764.4 $c=$ 576.9 $\beta=$ 90.54	4	180.2 187.5 180.3 188.7	217.1 214.5	140.6 146.4	−15	5.5	1.975	−0.65	AF	[4, 8]
$TlMnF_4$	$I2/a$	$a=$ 539.7 $b=$ 544.1 $c=$ 1248.4 $\beta=$ 90.19	4	177.6 186.1	214.6	146.5	− 1	2.3		−0.45	AF	[6]
$RbMnF_4$	$P2_1/a$	$a=$ 782.2 $b=$ 777.7 $c=$ 605.0 $\beta=$ 90.83	4	180.7 186.0 180.2 190.3	213.9 216.8	148.3 152.1	− 7	4.2	1.99	−0.275	AF	[4, 8]
$CsMnF_4$	$P4/n$	$a=$ 794.4 $c=$ 663.76	4	181.7 185.4	216.8	161.9	21	23	1.99	1.30	F	[3, 4, 8]

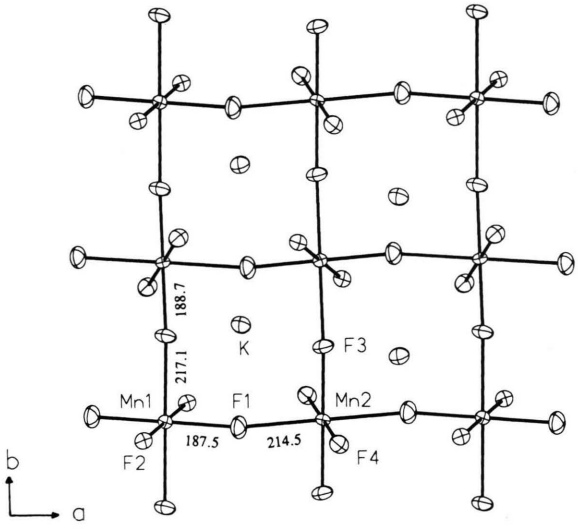

Fig. 14. Projection along [001] of a layer in $KMnF_4$. Thermal ellipsoids at 50% probability level.

especially through comparison with the related layer compounds $AFeF_4$ of the d^5-ion Fe^{3+}. For these 2-d magnetic systems with symmetrical Fe–F–Fe bridges the 2-d exchange energies J/k [31, 48] and the bridging angles β[49–52] were taken from the literature. In Fig. 15 the exchange energies are plotted for both systems of layered structures versus $\cos^2\beta$, where β means the average M–F–M bridging angle. Such a linear evolution of J/k with $\cos^2\beta$ has already been reported for the Mn^{3+} chain compounds [7], and can be described in the present case by the equation

$$J/k\,(\mathrm{Mn}) = 7\cos^2\beta - 5.2\,. \qquad (8)$$

The sign of J/k turns over at $\beta_c = 150°$, i.e. the antiferromagnetic ordering changes continuously into a ferromagnetic coupling of the moments. For better comparison of both d^4 and d^5 systems the results of the Fe(III) compounds have been rescaled for a hypothetic $S=2$ case simulating the properties of a d^4 system quasi without a Jahn-Teller effect.

Possible Exchange Pathways

The main difference in the J/k versus $\cos^2\beta$ functions for the Mn(III) and the Fe(III) compounds, the change in sign of the slope, may clearly be attributed to the principal difference in the dominating σ-superexchange mechanism between a d^4 Jahn-Teller system with antiferrodistortive ordered planes and a non

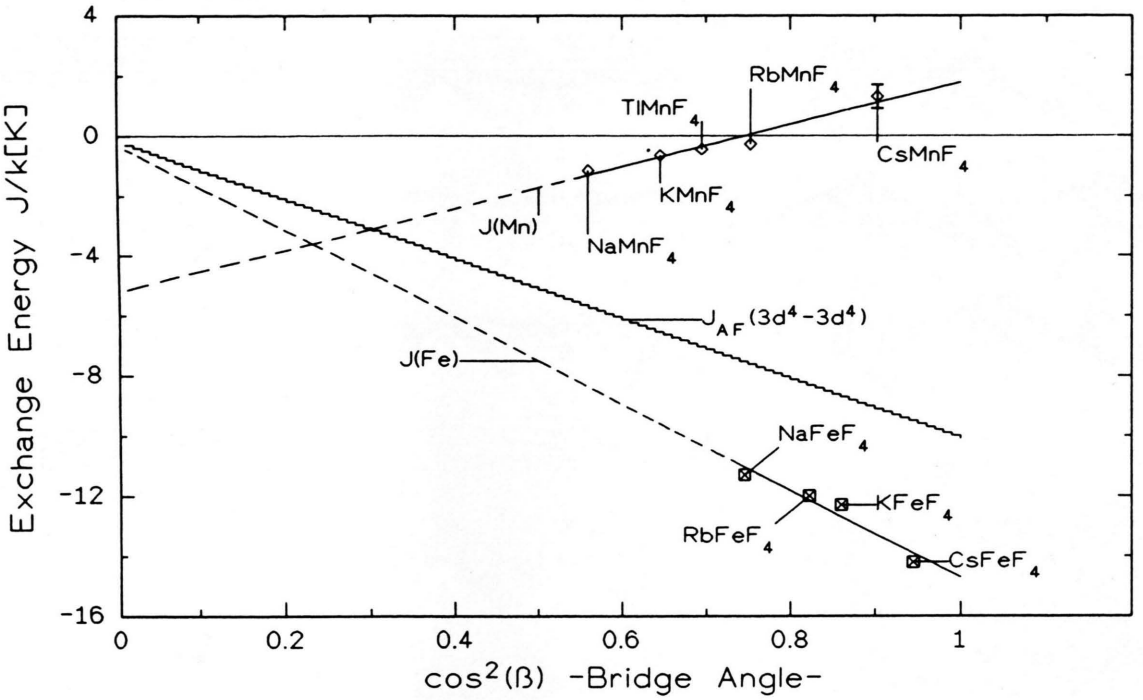

Fig. 15. Correlation between exchange energy J and bridge angle β.

Jahn-Teller d^5 system. According to the Goodenough-Kanamori-Anderson rules [53–55] the σ^*/σ exchange integral in the asymmetric Mn–F... Mn bridge is *ferromagnetic*, in the symmetrical Fe–F–Fe bridge the σ/σ interaction is *antiferromagnetic*. The orbitals involved are

$$\text{Mn}-d^0_{x^2-y^2} \ldots \text{F}-2p_z^2 \ldots \text{Mn}-d^1_{z^2} \quad \text{ferromagnetic,} \tag{9a}$$

$$\text{Fe}-d^1_{z^2} \quad \ldots \text{F}-2p_z^2 \ldots \text{Fe}-d^1_{z^2} \quad \text{antiferromagnetic.} \tag{9b}$$

Both σ-interactions are expected to decrease with a bridge angle β decreasing from the ideal value of 180°. The good linearity of the J/k versus $\cos^2\beta$ plot in Fig. 15 as well as for the 1-d systems in [7] suggests that the exchange energies roughly follow the overlap integral of the σ-interaction. Other examples with similar angle dependencies have been discussed for dimers e.g. by Hay et al. [56] or Atanasov and Angelov [57].

The σ interactions (9) explain well the positive and negative slopes of the $J/k-\cos^2\beta$ functions in Figure 15. But the reason for the early change to antiferromagnetism in the Mn(III) system at about $\beta = 150°$ has still to be found. The following points may play a role:

1. e_g-mixing: Kanamori pointed out [58] that the ideal case of ferromagnetic interaction (9a), based on the orthogonality of the metal d-orbitals, may turn towards antiferromagnetic coupling by the lowering of symmetry when the bridge angle deviates from 180°. He assumed that by anharmonic terms in the vibronic coupling within the antiferrodistortively ordered layers a mixing of both orbital states occurs with the consequence of partial electron transfer from the d_z^2 towards the empty $d_{x^2-y^2}$ orbital. In this way an antiferromagnetic contribution to the exchange should be expected at lower bridge angles. If this mechanism holds, at the same time a decrease of asymmetry in the Mn–F... Mn bridges should be observed with decreasing β. In the crystal structures of the $AMnF_4$ compounds such a trend is not documented (Table 4). Thus, the e_g-mixing cannot play an important role.

2. π/π-interactions: Two pure π-interaction pathways, $d^1_{yz} \ldots p_y^2 \ldots d^1_{yz}$ and $d^1_{xz} \ldots p_x^2 \ldots d^1_{xz}$, should provide approximately angle independent antiferromagnetic contributions. Such an antiferromagnetic "background" of about −5 K would explain the shift of the $J/k-\cos^2\beta$ line of the Mn(III) system down the ordinate. On the other hand, the same effect must be

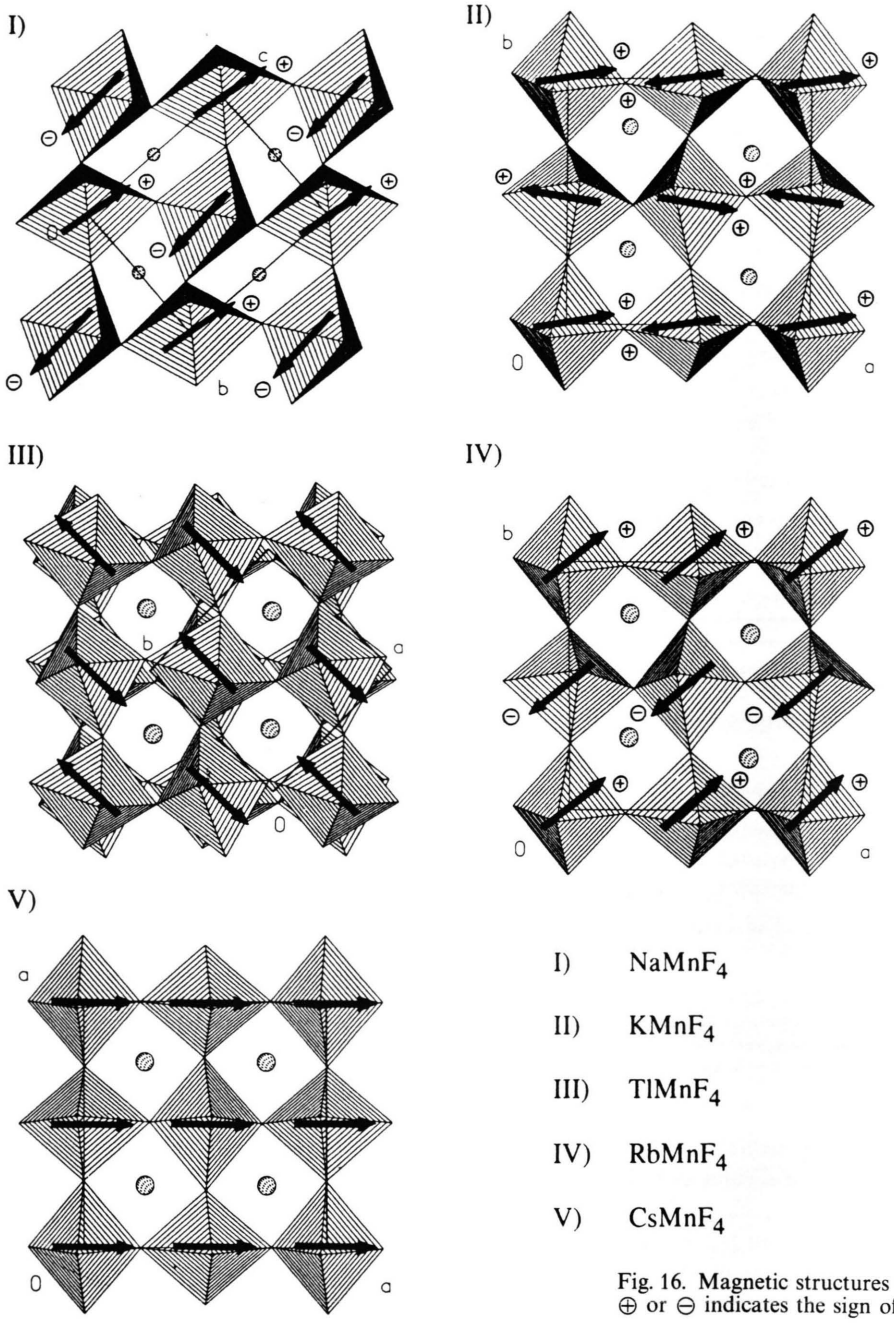

I) $NaMnF_4$

II) $KMnF_4$

III) $TlMnF_4$

IV) $RbMnF_4$

V) $CsMnF_4$

Fig. 16. Magnetic structures of $AMnF_4$.
⊕ or ⊖ indicates the sign of the M_z component.

assumed for the Fe(III) compounds where the line passes the zero point for $\beta = 90°$. The same is true for the function of the corresponding 1-d Mn(III) antiferromagnetic chain compounds. Thus, the contribution of such a π/π-interaction must be negligible. Taking the high distance dependence of π-interactions into account, this is not surprising, at least in the Mn(III) compounds, where long bonds (about 215 pm) are involved.

3. π/σ-interactions: $d^1_{xz} \ldots p_x \ldots d^1_{z^2}$. This interaction would be most effective at $\beta = 90°$. It may play an important role in the Mn(III) systems at lower

bridge angles when the π-interaction points along the short bond combined with the σ-interaction along the long bond. As the shorter Mn–F bonds (188 pm) of the asymmetric Mn–F... Mn bridges are much shorter than the Fe–F bonds in the symmetrical Fe–F–Fe bridges (196 pm), this type of interaction may give (due to the strong distance dependence of π-interactions) an important antiferromagnetic contribution for the Mn compounds only, but not for the Fe compounds.

4. s–d-mixing: $4s-3d_{z^2}$-mixing is assumed to explain the favouring of the elongation of MX_6-octahedra in strong Jahn-Teller systems (E_g ground state) [59, 60]. Its importance in our Mn(III) systems is documented in the large local anisotropy (about 3 K) connected with such a process. The consequence of the s–d-mixing for the superexchange interactions is an expansion of the d_{z^2}-orbitals. This effect provides good σ-overlap in spite of the large Mn ... F distance in the long part of Mn–F... Mn bridges. Thus both important exchange pathways, the σ^*/σ- and the π/σ-interaction are enhanced by this effect. Attempts for a more quantitative treatment of the exchange interactions and their angle dependence by the Angular Overlap Model and Ext. Hückel calculations have been performed by Atanasov. These results will be published separately [61].

Orientation of the Magnetic Moments in the $AMnF_4$ Compounds

As summarized in Fig. 16, the $AMnF_4$ compounds show four basic types of magnetic structure, all with spins approximately within the layer planes: $CsMnF_4$ is ferromagnetic with spins along *a* or *b* [3], $RbMnF_4$ is an antiferromagnet but along a where the bridge angle is 152°, the coupling is parallel, along *b* (angle 148°) it is antiparallel. In the Tl, K and Na compounds the coupling is antiparallel in both layer directions. The inter-layer coupling is ferromagnetic in $CsMnF_4$ and all other antiferromagnetic compounds except $NaMnF_4$, where it is antiferromagnetic like in the Fe compounds.

The direction of the spins in the antiferromagnetic compounds results as a compromise of the tendency for antiparallel spin orientation by the low exchange energies and the strong anisotropy. The out-of-plane anisotropy D_z clearly keeps the "easy" direction approximately within the layer plane where the long octahedral axes are oriented. The in-plane anisotropy D_x is less pronounced due to the antiferrodistortive ordering of the octahedra and the puckering of layers. Owing to the perpendicular ordering of the elongated axes, for a colinear spin array only one half of the spins can adopt the easy direction. Within the plane there are two comparable easy directions *a* and *b*. In $KMnF_4$ the a direction seems to get some preference. The small difference in susceptibilities along *a* and *b* of the single crystal (Fig. 12) and the problems in refining the magnetic structure from neutron diffraction data suggest anyhow the possible presence of magnetic domains with *b* orientation of spins. In $RbMnF_4$ and $TlMnF_4$, as a compromise between both easy directions, the diagonal spin orientation is preferred. The additional influence of puckering of the layers is supposed to be the reason for the observed canting in the Rb, K, and (from magnetization data) Na compounds. A Dzialoshinsky effect [62] is estimated to cause canting of less than about 1° and, thus, cannot explain our much larger effects.

Acknowledgements

We thank M. Atanasov for many helpful discussions. W.M. and M.M. thank the Commission of the European Communities for financial support (grant N° B/89000863). This work has been also supported by the Deutsche Forschungsgemeinschaft and the Fonds der Chemischen Industrie.

[1] (a) W. Massa, Inorg. Nucl. Chem. Lett. **13,** 253, (1977). (b) P. Köhler, W. Massa, D. Reinen, B. Hofmann, and R. Hoppe, Z. Anorg. Allg. Chem. **446,** 131 (1978).
[2] K. H. Wandner and R. Hoppe, Z. Anorg. Allg. Chem. **546,** 113 (1987).
[3] W. Massa and M. Steiner, J. Solid State Chem. **32,** 137 (1980)
[4] M. Molinier and W. Massa, Z. Naturforsch. **47b,** 783 (1992).
[5] M. Molinier, W. Massa, S. Khairoun, A. Tressaud, and J. L. Soubeyroux, Z. Naturforsch. **46b,** 1669 (1991).
[6] P. Nuñez, A. Tressaud, J. Grannec, P. Hagenmuller, W. Massa, D. Babel, A. Boireau, and J. L. Soubeyroux, Z. Anorg. Allg. Chem. **609,** 71 (1992).
[7] J. Pebler, W. Massa, H. Lass, and B. Ziegler, J. Solid State Chem. **71,** 87 (1987).
[8] M. Molinier, Thesis, Marburg, Germany, (1993)
[9] (a) H. M. Rietveld, Acta Cryst. **22,** 151 (1967). (b) H. M. Rietveld, J. Appl. Cryst. **2,** 65 (1969).
[10] (a) R. A. Young and D. B. Wiles, J. Appl. Cryst. **14,** 149 (1981). – (b) D. B. Wiles and R. A. Young, J. Appl. Cryst **15,** 430 (1982).

[11] J. Rodríguez-Carvajal, FULLPROF: a Program for Rietveld Refinement and Pattern Matching Analysis, Abstracts of the Satellite Meeting on Powder Diffraction of the XVth Congress of International Union of Crystallography, 127, Toulouse, France 1990.
[12] V. F. Sears, Neutron News **3**(3), 26 (1992).
[13] E. J. Lisher and J. B. Forsyth, Acta Cryst. **A27,** 545 (1971).
[14] J. Pebler, Z. Naturforsch. **31 b,** 1039 (1976).
[15] S. A. Wolf, J. R. Davis, and M. Nisenoff, IEEE Trans. Comm. Com. **22,** 549 (1974).
[16] (a) M. Hidaka, Z. Y. Zhou, and S. Yamashita, Phase Transitions **18**(1–2), 103 (1989). (b) L. J. Lewis, and Y. Lépine, Phys. Rev. B **40**(5), 3319 (1989). (c) A. Gibaud, H. You, S. M. Shapiro, and J. Y. Gesland, Phys. Rev. B **42** (13), 8255 (1990). (d) J. P. Toennies and R. Vollmer, Phys. Rev. B **44**(18), 9833 (1991).
[17] F. Palacio, M. C. Morón, and J. Rodríguez-Carvajal, in Spanish Scientific Research Using Neutron Scattering Techniques, Cantabria, Spain 1991.
[18] M. C. Morón, F. Palacio, and J. Rodríguez-Carvajal, Physica B **180 & 181,** 125 (1992).
[19] M. Molinier, W. Massa, S. Khairoun, A. Tressaud, A. Boireau, and J. L. Soubeyroux, J. Fluor. Chem. **54** (1–3) Compl. Vol. 54, 411 (1991).
[20] M. C. Morón, F. Palacio, and J. Rodríguez-Carvajal, J. Appl. Phys. **73** (10), 6540 (1993).
[21] M. C. Morón, F. Palacio, and J. Rodríguez-Carvajal, J. Phys.: Codens. Matter **5,** 1 (1993).
[22] (a) F. Rodriguez, M. Moreno, J. M. Dance, and Tressaud, Solid State Commun. **69** (1), 67 (1989). (b) U. J. Cox, R. A. Cowley, S. Bates, and L. D. Cussen, J. Phys.: Condens. Matter **1,** 3031 (1989).
[23] C. Frommen and J. Pebler, to be published.
[24] G. Heger, R. Geller, and D. Babel, Solid State Commun. **9,** 335 (1971).
[25] G. Heger and R. Geller, Phys. Stat. Sol. B **53**, 227 (1972).
[26] J. D. Rush, A. Simopoulos, M. F. Thomas, and B. M. Wanklyn, Solid State Commun. **18,** 1039 (1976).
[27] M. Eibschütz, G. R. Davidson, and H. J. Guggenheim, Phys. Rev. B **9** (9), 3885 (1974).
[28] M. Eibschütz, H. J. Guggenheim, and L. Holme, J. Appl. Phys. **42,** 1485 (1971).
[29] K. Kopitzki, in Einführung in die Festkörperphysik; 2. Aufl.; Teubner, B. G., Ed.; Stuttgart 1989.
[30] F. Keffer, in Handbuch der Physik; Band 18/2; Springer-Verlag, Berlin 1966.
[31] L. J. de Jongh and A. R. Miedema, Adv. Phys. **23,** 1 (1974).
[32] C. E. Johnson, in Mössbauer Spectroscopy Applied to Inorganic Chemistry; Long, G., Ed.; Plenum Press, New York (1984), Vol. 1.
[33] J. Pebler and F. W. Richter, Z. Physik **221,** 480 (1969).
[34] W. Massa, J. Pebler, F. Hahn, and D. Babel, in "Organic and Inorganic Low-Dimensional Crystalline Materials", NATO ASI Series B: Physics **168,** 429, Plenum Press, New York 1987.
[35] L. J. de Jongh, J. Appl. Phys. **53,** 8018 (1982), and references therein.
[36] T. H. R. Skyrne, Proc. Roy. Soc. London **262,** 237 (1961).
[37] F. Waldner, Proc. XXII Congress Ampère, Zürich 1984, p. 147.
[38] F. Waldner, J. Magn. Magn. Mat. **31–34,** 1203 (1983).
[39] J. Pebler, Inorg. Chem. **28,** 1038 (1989).
[40] H. J. DeGroot, Thesis, Leiden, The Netherlands 1986.
[41] H. M. A. Smit, Thesis, Leiden, The Netherlands 1988.
[42] (a) G. S. Rushbrooke and P. J. Wood, Molec. Phys. **1,** 257 (1958). (b) G. S. Rushbrooke and P. J. Wood, Molec. Phys. **6,** 409 (1963).
[43] M. E. Lines, J. Phys. Chem. Solids **31,** 101 (1970).
[44] J. H. P. Colpa, E. G. Sieverts, and R. H. Van der Linde, Physica **51,** 573 (1971).
[45] H. A. Groenendijk, A. J. Van Duyneveldt, and R. D. Willett, Physica **98 B,** 53 (1979).
[46] D. J. Breed, Physica **37,** 35 (1967).
[47] L. J. de Jongh (Ed.), Magnetic Properties of Layered Transition Metal Compounds, Kluwer Academic Publishers, Dordrecht 1990.
[48] A. Tressaud and J. M. Dance, Structure and Bonding **52,** 87 (1982).
[49] D. Babel, F. Wall, and G. Heger, Z. Naturforsch. **29 b,** 139 (1974).
[50] J. M. Dance, A. Tressaud, W. Massa, and D. Babel, J. Chem. Research (S), 202 (1981).
[51] (a) J. Lapasset, P. Sciau, J. Moret, and N. Gros, Acta Cryst. **B42,** 258 (1986). (b) J. Lapasset, P. Sciau, J. Moret, and N. Gros, Acta Cryst. **B43,** 111 (1987).
[52] M. C. Morón, A. Bulou, C. Pique, and J. L. Fourquet, J. Phys.: Condens. Matter **2,** 8269 (1990).
[53] J. B. Goodenough, in Magnetism and the Chemical Bond, Interscience Publishers, John Wiley & Sons, New York 1963.
[54] J. Kanamori, J. Phys. Chem. Solids **10,** 87 (1959).
[55] P. W. Anderson, Phys. Rev. **79,** 350 (1950).
[56] P. J. Hay, J. C. Thibeault, and R. Hoffmann, J. Am. Chem. Soc. **97,** 4884 (1975).
[57] M. Atanasov, S. Angelov, and I. Mayer, J. Molec. Struct. (Theochem) **187,** 23 (1989).
[58] J. Kanamori, J. Appl. Phys. Suppl. **31,** 14 (1960).
[59] R. Hoffmann, Science **211,** 995 (1981).
[60] J. Burdett, Inorg. Chem. **20,** 1959 (1981).
[61] M. Atanasov, to be published.
[62] I. E. Dzialoshinsky, J. Phys. Chem. Solids **4,** 241 (1958).